IOP Publishing Journal of Physics D: Applied Physics
J. Phys. D: Appl. Phys. **00** (2016) 000000 (7pp) UNCORRECTED PROOF

Insulator-to-metal transition in vanadium supersaturated silicon: variable-range hopping and Kondo effect signatures

E García-Hemme, D Montero, R García-Hernansanz, J Olea, I Mártil and G González-Díaz

Departamento de Física Aplicada III (Electricidad y Electrónica), Univ. Complutense de Madrid, 28040 Madrid, Spain

AQ1 E-mail: xxxx

Received 10 March 2016
Accepted for publication 12 May 2016
Published

Abstract

We report the observation of the insulator-to-metal transition in crystalline silicon samples supersaturated with vanadium. Ion implantation followed by pulsed laser melting and rapid resolidification produce high quality single-crystalline silicon samples with vanadium concentrations that exceed equilibrium values in more than 5 orders of magnitude. Temperature-dependent analysis of the conductivity and Hall mobility values for temperatures from 10 K to 300 K indicate that a transition from an insulating to a metallic phase is obtained at a vanadium concentration between 1.1×10^{20} and 1.3×10^{21} cm^{-3}. Samples in the insulating phase present a variable-range hopping transport mechanism with a Coulomb gap at the Fermi energy level. Electron wavefunction localization length increases from 61 to 82 nm as the vanadium concentration increases in the films, supporting the theory of impurity band merging from delocalization of levels states. On the metallic phase, electronic transport present a dispersion mechanism related with the Kondo effect, suggesting the presence of local magnetic moments in the vanadium supersaturated silicon material.

Keywords: insulator-to-metal transition, ion implantation, Kondo effect, variable range hopping, pulsed laser annealing

S Online supplementary data available from stacks.iop.org/JPhysD/00/0000/mmedia

AQ2 (Some figures may appear in colour only in the online journal)

1. Introduction

Research on the insulator-to-metal transition in the condensed-matter systems has always been a fruitful field. Especially important is the transition to the insulating phase caused by the correlation effects associated with the electron-electron interaction [1]. In the metallic phase near the transition point it has been observed fluctuations and orderings in the spin, charge, and orbital degrees of freedom, properties which are frequently quite different from those of ordinary metals [2, 3]. The insulator-to-metal transition could be driven by means of control of key parameters such as band filling or energy bandwidth. These parameters are experimentally varied by doping, pressure, chemical composition, and magnetic fields [4–6]. Particularly the insulator-to-metal transition controlled by doping depends on a critical doping concentration (n_{crit}) which for a variety of systems satisfies $a_b\, n_{crit}^{1/3} = 0.25$ [7], where a_b is the effective Bohr radius of the dopant impurity.

Silicon, as the key material of the information era and a technological mature material has been an accessible playground in order to explore the fundamentals of the insulator-to-metal transition phenomena. We are referring to the insulator-to-metal transition in silicon at low temperatures (under 50 K), at which silicon behaves as an insulator material due to the freeze out effect [8]. Most of the insulator-to-metal transitions driven by doping in silicon have been studied

JNL:JPD PIPS: AA26D1 TYPE: PAP TS: NEWGEN DATE:24/5/16 EDITOR: IOP SPELLING: US

using shallow dopants such as phosphorous or boron which present a Bohr radius on the order or 10 nm and a theoretical $n_{crit} \approx 10^{18}$ cm^{-3}. This theoretical n_{crit} is in good agreement with experimental values [9]. These shallow dopants present high solubilities in silicon (higher than n_{crit}), which permits to obtain high quality metallic and insulating samples using traditional equilibrium growth techniques. However, deep levels impurities present more tightly bound electrons and therefore n_{crit} is expected to be higher than in the case of shallow dopants. Transition metals in silicon produce deep levels and present much lower equilibrium solubilities ($\approx 10^{15}$ cm^{-3}) than shallow dopants. In fact, the n_{crit} that determines the insulator-to-metal transition for deep level impurities has been theoretically calculated to be approximately 6×10^{19} cm^{-3} [10]. This value is in agreement with experimental results [11, 12]. Consequently, equilibrium process techniques does not permit to produce adequate samples to study an insulator-to-metal transition in silicon supersaturated with transition metals and an exhaustive analysis of this phenomena has not been previously reported. In this work, in order to overcome the challenge of supersaturation (concentration higher than equilibrium solubility) in high quality crystalline samples we use non-equilibrium process techniques as ion implantation and pulsed laser melting (PLM) [13].

Recent studies based on Si supersaturated with chalcogens [12, 14], titanium [15] and vanadium [16] have shown a wide range of unusual electrical and optical properties, namely, a strong sub bandgap optical absorption and an increase in the infrared photo-response. One of the hypotheses to explain these properties is the formation of an impurity band of allowed states within the bandgap of the host semiconductor once the impurity concentration has overcome the so-called insulator-metal transition. This impurity band would allow optical transitions for photon energies below the bandgap which, together with a recovery of the carrier lifetime, would lead to an increase in the photo-response at these photon energies. In this context, these materials are currently studied for potential photovoltaic applications since the exploitation of the infrared region of the solar spectrum in Si-based solar cells is a goal for the photovoltaic researchers. The concept of a solar cell based on this impurity band material is known as intermediate band solar cell (IBSC) and would lead to a remarkable increase in the solar cell efficiency [17, 18].

This work focuses on the electrical transport properties in the low temperature range and studies the insulator-to-metal transition occurring in silicon supersaturated with vanadium and controlled by the impurity concentration. This analysis allows us to add novel results to the research field of the transition-metal supersaturated silicon materials: the identification of a variable-range hopping transport for insulating samples and a scattering mechanism driven by the Kondo effect for metallic samples.

2. Experimental

Single-crystal samples 1×1 cm^2 in size of n-type Si (1 1 1) with a thickness of 300 μm ($\rho \approx 200$ Ω cm; $\mu \approx 1500$ cm^2 V^{-1} s^{-1}; $n \approx 2.2 \times 10^{13}$ cm^{-3} at room temperature) were implanted in a refurbished VARIAN CF3000 Ion Implanter at 32 keV with ^{51}V$^+$ at 4 different doses (10^{13}, 10^{14}, 10^{15} and 10^{16} cm^{-2}) using a 7° tilt angle. After implantation, all the samples were PLM processed at 1 J cm^{-2} with a KrF excimer laser (248 nm) with a 20 ns pulse duration at IPG Photonics (New Hampshire, USA).

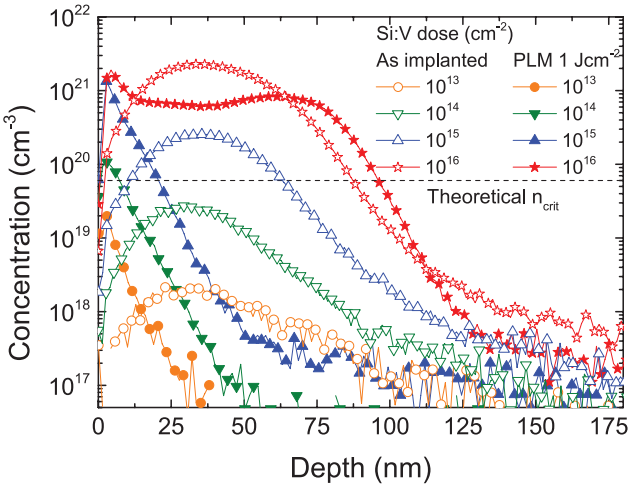

Figure 1. ToF-SIMS profiles of V-implanted samples with the four implantation doses (10^{13}, 10^{14}, 10^{15} and 10^{16} cm^{-2}). Profiles are presented for the as-implanted samples (empty symbols) and for the subsequently laser processed at 1 J cm^{-2} samples (full symbols).

To analyze the vanadium depth profile, time-of-flight secondary ion mass spectrometry (ToF-SIMS) measurements were carried out in a ToF-SIMS IV model manufactured by ION-TOF, with a 25 keV pulsed Bi^{3+} beam at 45° incidence. A 10 keV voltage was used to extract the secondary ions and their time of flight from the sample to the detector was measured with a reflection mass spectrometer. The structural characterization of similar samples was carried out by high resolution transmission electron microscopy (TEM) images, obtained with a Titan3 G2 working at 300 keV.

Electrical characterization was made at variable temperature (10–300 K) placing the samples inside a closed-cycle Janis cryostat. A Keithley SCS 4200 model with four source and measure units (SMU) was used to perform sheet conductance and Hall effect measurements with the van der Pauw configuration. Details on the electrical characterization setup can be found elsewhere [19].

3. Results

Figure 1 shows the V concentration depth profiles obtained by ToF-SIMS for samples implanted with the four different doses. Profiles are shown for the as-implanted samples and for the subsequently PLM processed samples. The theoretical n_{crit} (theoretical concentration limit to overcome the insulator-to-metal transition) is plotted as a reference. We can observe that for all the different PLM processed samples we have obtained silicon supersaturated films with vanadium concentrations higher than 10^{15} cm^{-3} which is the vanadium solubility limit in silicon. Comparing the as-implanted

Table 1. Peak vanadium concentration (c_{peak}), thickness layer (t_{crit}) with a vanadium concentration over the theoretical n_{crit}, and remaining dose for samples implanted with the four doses (10^{13}, 10^{14}, 10^{15} and 10^{16} cm^{-2}) and subsequently PLM processed at 1 J cm^{-2}.

Implantation dose (cm^{-2})	10^{13}	10^{14}	10^{15}	10^{16}
c_{peak} (cm^{-3})	1.98×10^{19}	1.07×10^{20}	1.33×10^{21}	1.89×10^{21}
t_{crit} (nm)	—	7	21	96
Remaining dose (cm^{-2})	7.6×10^{12}	8.1×10^{13}	8.3×10^{14}	6.4×10^{15}

profiles with the subsequently PLM processed profiles we can observe an important redistribution of the vanadium atoms due to the PLM process. For samples implanted with the 10^{13}, 10^{14} and 10^{15} cm^{-2} doses, the implanted profile is pushed towards the surface of the sample while the concentration peak increases as the implantation doses increase. This behavior is known as snow-plow effect and is a second order consequence of the PLM process [20]. The laser process melts the implanted layer up to a certain depth. Then, the solidification process begins from this depth towards the surface of the layer. In this process, the melting front moves towards the surface at velocities of several meters per second, in a process known as explosive recrystallization. Implanted impurities tend to stay in the liquid phase since the solubility limit is higher. Consequently, the melting front pushes the impurities towards the surface and shows the characteristic depth-profiles presented in figure 1.

However, for the sample implanted with the highest dose of 10^{16} cm^{-2} we observe that the maximum peak concentration does not surpass the value obtained for the sample implanted with the 10^{15} cm^{-2} dose, which shows an in depth box-shaped profile. In order to explain this observation we should point out that the laser depth penetration is directly related with the amorphization degree in the sample [21]. The sample implanted with the dose of 10^{16} suffered a higher degree of amorphization and consequently the laser treatment melted a larger depth in the implanted layer. Impurities in the melted region tend to spread out uniformly since the solubility and diffusion coefficients are higher in the liquid phase. Therefore, an in depth box-shaped profile appears. The larger the laser penetration depth, the larger the box-shaped profile is and the lower the maximum concentration is, since impurities have to spread out in a larger volume of material [21, 22]. When the recrystallization process starts, lots of impurities are trapped in the solid phase while others are pushed towards the surface by the snow-plow effect [20]. For this reason, we also observe how the concentration profile increases as we move towards the surface of the layer.

Analysis of figure 1 suggests that there is a concentration limit for the supersaturation process that is impossible to overcome, even with the use of non-equilibrium techniques. The most remarkable result shown in figure 1 is that the theoretical n_{crit} has been clearly exceeded for the 10^{15} cm^{-2} implanted sample in a layer of ~21 nm and for the 10^{16} cm^{-2} implanted sample in a layer of ~96 nm. The sample implanted with a dose of 10^{13} cm^{-3} presents a vanadium concentration below the theoretical n_{crit} while the sample implanted with a dose of 10^{14} cm^{-3} presents a concentration slightly higher than the theoretical n_{crit} limit, but just in an extremely thin layer (~7 nm).

Table 1 summarize the main results extracted from the analysis of figure 1, showing the peak concentration (c_{peak}), layer thickness (t_{crit}) having a vanadium concentration over the theoretical n_{crit}, and the remaining implanted dose after the PLM process. The remaining dose after the PLM process was calculated by the numerical integration of the depth profile. The remaining dose indicates a vanadium loss in the 17–36% range due to the nature of the PLM process, which tends to expel a certain amount of implanted impurities during the crystallization process.

Crystalline quality of the implanted and PLM processed layers were analyzed using high resolution TEM images shown in figure 2. We can observe the excellent crystalline quality obtained for samples implanted with 10^{13}, 10^{14} and 10^{15} cm^{-2} doses, virtually indistinguishable from a silicon reference sample. This result is significant, particularly for the sample implanted with the 10^{15} cm^{-2} dose since we have obtained a supersaturated silicon sample with vanadium concentration high enough to theoretically undergone the insulator-to-metal transition and in a high quality single crystal. This high crystal quality has been also confirmed in other silicon supersaturated materials by means of Rutherford–Backscattering experiments [23]. However, for the sample implanted with the highest dose of 10^{16} cm^{-2} we observe a branching structure that cross the processed layer. In low magnification images (images not shown) [16], we observe a set of these branching filamentary structures across the entire processed layer. These nanoscale features referred to as cellular-breakdown [24, 25] (due to the presence of surface features resembling cell walls in plants). In a recent work, the 3D structure and composition of Si cellular-breakdown structures formed in a similar material have been investigated using atom probe tomography technique [26]. In this work, it has been shown that these filamentary structures are formed by transition metals segregation regions with up to a 10 $^{a}/_{o}$ in Si. In any case, these structures resulted free of defects presenting no evidence of polycrystalline material neither the formation of silicides [26, 27].

From the analysis of the integrated ToF-SIMS profile we deduced that a certain amount of the implanted vanadium is expelled during the crystallization process. However, we have never observed in XTEM images (figure 2) a thin layer of pure vanadium on top of the supersaturated silicon layer. Therefore, we suggest that the expelled vanadium suffers a sublimation process due to the laser treatment and evaporates.

Figure 3 shows the temperature dependence of the sheet conductance (G_s) for an unprocessed silicon sample used as a reference and for the vanadium supersaturated silicon samples with the 4 different implantation doses and subsequently PLM annealed. Sheet carrier concentration (n_s) values for these samples are shown in the inset graph for the low temperature

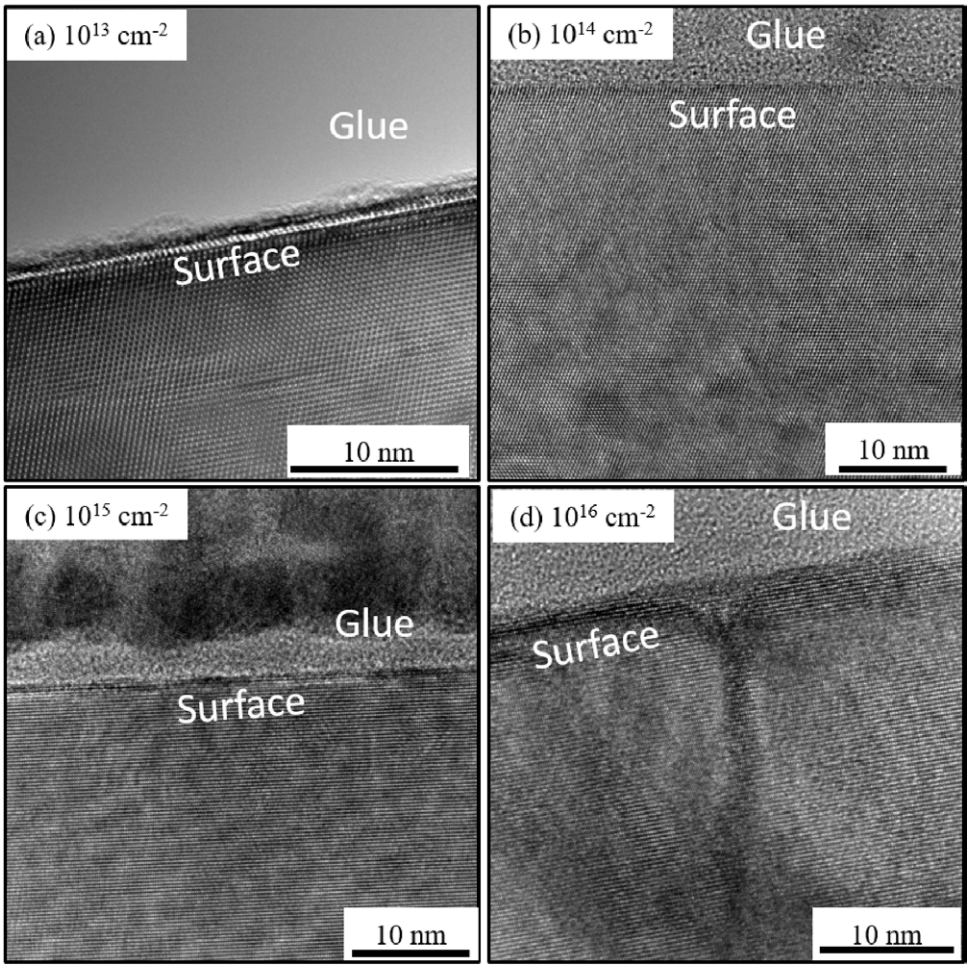

Figure 2. High resolution TEM images of the vanadium supersaturated silicon layers implanted with the doses of 10^{13} (a), 10^{14} (b), 10^{15} (c) and 10^{16} cm^{-2} (d). All samples were subsequently PLM annealed with an energy laser density of 1 J cm^{-2}.

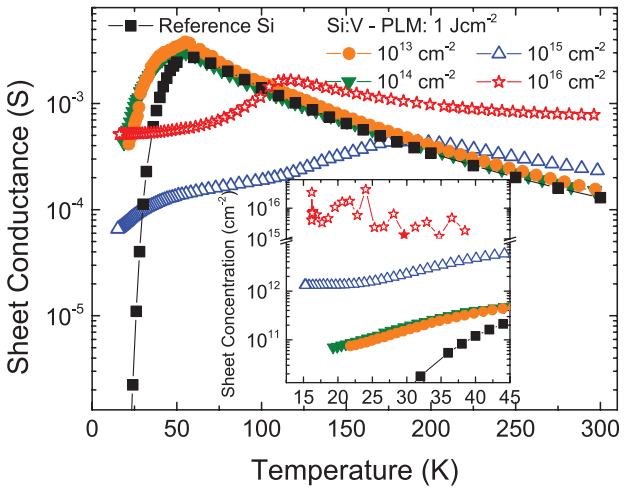

Figure 3. Temperature dependence of the sheet conductance for the silicon reference sample and for the vanadium supersaturated silicon samples implanted with the four doses (10^{13}, 10^{14}, 10^{15} and 10^{16} cm^{-2}), subsequently PLM annealed at 1 J cm^{-2}. Inset presents the temperature dependence of the sheet carrier concentration for the same samples.

range. The silicon unimplanted sample presents the expected behaviour, that is an abrupt increase of the G_s from 10 to 50 K due to the carriers freeze-out effect and a decrease of the G_s as the temperature increases from 50 to 300 K due to the increase of the phonon scattering.

Samples implanted with the lowest doses of 10^{13} and 10^{14} cm^{-2} present a behavior similar to that of the unimplanted silicon sample for temperatures higher than 60 K. We can identify differences in the freeze-out temperature range, at which both samples present G_s and n_s values higher than those of the unimplanted silicon (up to three orders of magnitude). Due to these high differences we can confirm that the underneath Si substrate is not participating in the transport at these low temperatures. This characteristic would be due to the presence of deep-levels introduced by the vanadium atoms. Later we deeply analyze this feature.

Samples implanted with the highest doses of 10^{15} and 10^{16} cm^{-2} present a completely different behavior. For temperatures higher than 200 K (10^{15} cm^{-2} sample) and 100 K (10^{16} cm^{-2} sample) the G_s values are higher than those of the silicon reference sample. For lower temperatures G_s decreases for both samples and presents lower values than the G_s of the silicon reference sample, until the substrate reaches the freeze-out effect, where the tendency is reversed. These features have been analyzed and explained in [11, 19], in the framework of a bilayer structure formed by a material with a semi-filled band within the silicon bandgap, known as intermediate band (IB) material [17, 28], and the underneath Si substrate. In these

[11, 19], the IB layer was obtained from the process of delocalization of the deep-levels of titanium in supersaturated silicon samples that have undergone the insulator-to-metal transition. At high temperatures, the bilayer structure is electrically coupled and electrical transport is performed through both layers in parallel (the IB material and the underneath Si substrate). But at low temperatures a decoupling process isolates the IB layer (implanted) from the silicon substrate and conduction happens only through the IB layer [19]. This decoupling process cannot be associated to implantation/PLM induced structural defects, since high resolution TEM images shown in figure 2 present a very high crystal quality after the PLM. The isolation process is dramatically notable at low temperatures, where the abrupt freeze-out effect experienced by the silicon substrate produces changes neither in the G_s nor in the n_s values of samples implanted at the highest doses. This confirms that the underneath silicon substrate is not playing any role in the transport at low temperatures. Moreover, for temperatures below 25 K these samples present a temperature-independent n_s value, as expected for an impurified semiconductor in the metallic phase [29]. We thus conclude that layers implanted with 10^{13} and 10^{14} cm^{-2} doses are in the insulating phase, whereas samples implanted with 10^{15} and 10^{16} cm^{-2} are in the metallic phase.

4. Discussion

Layers in the metallic phase would present an IB produced by the delocalization of the electrons belonging to the vanadium atoms. At low temperatures ($T < 25$ K), metallic electrical transport is driven through the IB. Values of n_s for these samples obtained in the inset of figure 3 would give us information about the band-filling. Taking into account t_{crit}, we calculated a charge carriers concentration of 6.6×10^{20} cm^{-3} for the sample implanted with 10^{16} cm^{-2} and a lower band-filling of 6.2×10^{17} cm^{-3} for the sample implanted with 10^{15} cm^{-2}. In the next part of the discussion we analyze the insulator-to-metal transition for all the implanted samples at low temperatures, where the underneath silicon substrate is not participating since it has undergone the freeze-out effect.

Up to this point, we have been using the sheet conductance (G_s) results, which are the values that are directly obtained from the measurements. We will develop the next part of the discussion in terms of conductivity, $\sigma(T)$. Both parameters are just related by the conduction thickness. We should note that at low temperatures, the conduction thickness is just the thickness of the vanadium supersaturated silicon layer (thermally constant), since the underneath silicon substrate undergoes the freeze-out effect.

At low enough temperatures electrical transport in the insulating phase can only be achieved through the localized deep-levels in a transport process known as hopping [30]. Under these conditions, the conductivity scales as:

$$\sigma(T) = \sigma_0 \exp\left[-(T_0/T)^s\right] \tag{1}$$

Where the s parameter defines the different hopping transport regimes and σ_0 and T_0 are parameters related with the microscopic material properties. Both have different expressions depending on the value of s [31]. In contrast, once we overcome the transition to the metallic phase the conductivity can be modelled by the potential law [32]:

$$\sigma(T) = \sigma(0) + CT^z \tag{2}$$

Where $\sigma(0)$ represents the 0 kelvin conductivity, C is a constant and z defines the scattering mechanism in the metallic phase. Usually z takes a value of 1/2 which describes the electron-electron scattering at low temperatures [33]. Zabrodskii and Zinoveva [31] introduced a useful procedure in order to identify if a material is in a metallic or an insulating phase. The procedure consists in defining the function $W(T)$:

$$W(T) = \frac{\mathrm{d}\ln\sigma}{\mathrm{d}\ln T} = \left(\frac{T}{\sigma}\right)\frac{\mathrm{d}\sigma}{\mathrm{d}T} \tag{3}$$

For materials in the insulating phase, inserting equation (1) in equation (3) gives

$$W(T) = s\left(\frac{T_0}{T}\right)^s \tag{4}$$

That is, function $W(T)$ should tend to infinity as temperature decreases for samples in the insulating phase. Performing the same procedure for materials in the metallic phase, introducing equation (2) in equation (3) gives

$$W(T) = \frac{zCT^z}{[\sigma(0) + CT^z]} = \frac{zCT^z}{\sigma(T)} \tag{5}$$

In this case, if the material exhibit a non-zero conductivity at $T = 0$ K, then function $W(T)$ should extrapolate to zero as temperature tend to zero K. Behavior of function $W(T)$ is presented in figure S1 in the supplemental material stacks.iop.org/JPhysD/00/0000/mmedia [34] and supports the conclusion extracted from figure 3. Equation (1) describes the transport properties in the insulating phase with values of s parameter describing the different hopping process. $s = 1$ is related to a nearest-neighbour hopping, $s = 1/4$ corresponds to Mott's variable-range hopping and $s = 1/2$ describes a variable-range hopping process with a Coulomb gap in the density of states [35, 36]. To identify the value of s we plotted log W versus log T (from equation (4)), being the slope of the data-fit equal to the value of $-s$. We obtained a value of $s = 0.56 \pm 0.21$ for the sample implanted with the dose of 10^{14} cm^{-2} and a value of $s = 0.75 \pm 0.58$ for the sample implanted with the lowest dose of 10^{13} cm^{-2}. Unfortunately, these values present large error bars. Therefore, we can only use this result as a first approximation to suggest the kind of underlying hopping process in these samples. 's' values are closer to 1/2 indicating that conduction likely occurs by variable-range hopping with a Coulomb gap in the density of states [35]. Hopping transport is most likely to occur in the freeze-out regime of an impurified semiconductor, in agreement with the previous suggestion. However, we must leave the door open for a more precise calculation of the kind of transport.

Figure 4(a) presents the logarithmic scale of G_s values as a function of $T^{-1/2}$ as well as the fit to equation (1) describing a variable-range hopping process with a Coulomb gap in the density of states for insulating samples. It is important to note

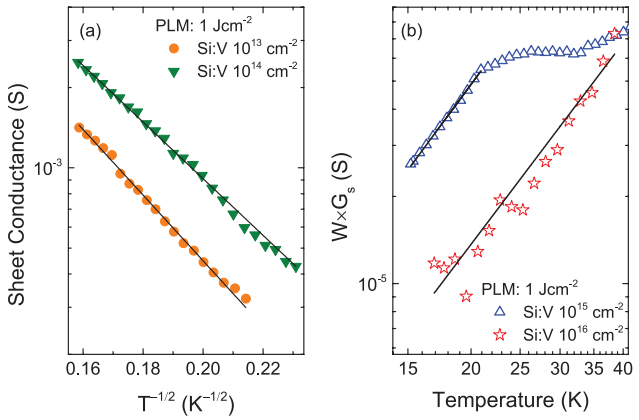

Figure 4. Analysis of transport properties for (a) samples in the insulating phase (implanted with the doses of 10^{13} and 10^{14} cm^{-2}) showing the sheet conductance values as a function of $T^{-1/2}$ and fits to equation (1). Panel (b) presents the analysis for samples in the metallic phase (implanted with the doses of 10^{15} and 10^{16} cm^{-2}) showing the product $W \times G_s$ as a function of the temperature as well as fits to equation (5).

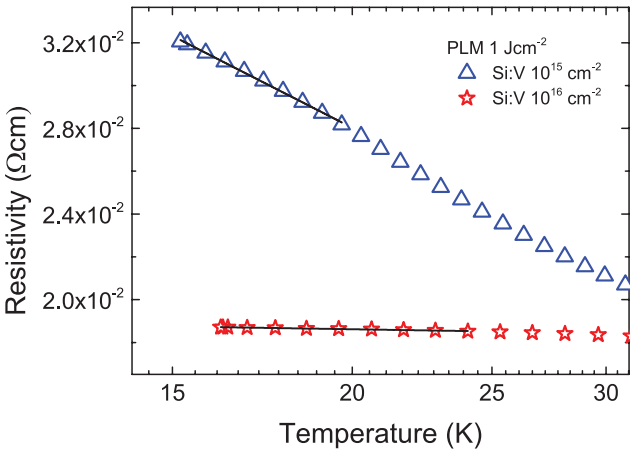

Figure 5. Resistivity as a function of temperature for samples in the metallic phase (implanted with the doses of 10^{15} and 10^{16} cm^{-2} and subsequently annealed at 1 J cm^{-2}). Fits to Kondo original dependence are also presented: $\rho(T) \approx -J\ln(T)$.

that the temperature region selected to perform the linear fit has been chosen to assure that since the silicon substrate has undergone the freeze-out effect (18–40 K), therefore it is not playing any role. According to Efros and Shklovskii [35], the characteristic parameter T_0 (equation (1)) is related with fundamentals material properties: $T_0 = 2.8q^2/\varepsilon k_B \xi$, where q is the electron charge, ε is the material permittivity, k_B is the Boltzmann constant and ξ is the electron wavefunction localization length. From data fitting we obtained a $T_0 = 802$ K for the sample implanted with 10^{13} cm^{-2} and a $T_0 = 596$ K for the sample implanted with 10^{14} cm^{-2}. Using a permittivity value for silicon of 1.06×10^{-10} Fm^{-1} [8] we calculated the localization lengths for both samples, corresponding to 61 nm for the sample implanted with a dose of 10^{13} cm^{-2} and a higher localization length of 82 nm for the sample implanted with a dose of 10^{14} cm^{-2}. These localization length values are in the same order as values obtained in the analysis of a polycrystalline silicon thin film transistor [37]. The result that the wavefunction tends to delocalize (increase of localization length) as the vanadium concentration increases is significant since supports the theory of impurity band merging from deep-levels delocalization process [10].

Finally we present the electrical transport analysis in the metallic phase for samples implanted with the doses of 10^{15} and 10^{16} cm^{-2}. Figure 4(b) shows the product $W \times G_s$ as a function of the temperature as well as fits to the equation (5). We should note that linear fit have been performed in the sample implanted with a dose of 10^{15} cm^{-2} just in the temperature range where we have confirmed the metallic phase, that is, from 14 to 24 K. We already confirmed this result in the inset of figure 3 where we observed a temperature-independent sheet carrier concentration for this temperature range, as well as in figure S1(b) [34], where the function $W(T)$ clearly extrapolates to zero as the temperature decreases in the same range. For the sample implanted with the dose of 10^{16} cm^{-2} we had chosen a higher temperature range (15–38 K) for the same reasons stated above. From the fits to equation (5) we obtained a value of $z = 2.33 \pm 0.03$ for sample implanted with a dose of 10^{15} cm^{-2} and a similar value of $z = 2.31 \pm 0.15$ for sample implanted with a dose of 10^{16} cm^{-2}. These values are close to $z = 2$, which is related to the Kondo effect, a scattering process due to the presence of local magnetic moments [38, 39]. This evidence has not been yet observed in any silicon supersaturated material. Vanadium atoms present an electronic configuration of (Ar) $3d^3 4s^2$. Therefore, we suggest that the unpaired d-electrons of vanadium atoms would be the origin of the presence of local magnetic moments.

Moreover, in Kondo's original paper [40], the local magnetic moments scattering was derived as $\rho(T) \approx -J\ln(T)$, where $\rho(T)$ is the resistivity and J is a prefactor directly proportional to the concentration of magnetic impurities responsible for the scattering phenomena. In figure 5 we present the resistivity-temperature values for samples in the metallic phase as well as fits to Kondo original dependence. From the fits we have obtained values for J of 14.9×10^{-3} for the sample implanted with 10^{15} cm^{-2} and 0.46×10^{-3} for the sample implanted with the highest dose of 10^{16} cm^{-2}. At least initially, this result seems contrary to the hypothesis that vanadium atoms are responsible for the magnetic impurities scattering, since the sample with a higher dose of remaining vanadium presents a lower scattering prefactor J. However, if we carefully analyze the band-filling results previously discussed we can conclude that in fact, the sample implanted with the dose of 10^{15} cm^{-2} presents a much higher concentration of vanadium atoms with respect to the charge carriers concentration and therefore could be suffering a proportionally higher scattering of magnetic impurities centers. Substracting the sheet carriers concentration values at low temperatures from the remaining dose and taking into account the t_{crit}, we calculated the concentration of vanadium atoms that would be contributing to the magnetic scattering. We obtained a value of 1.04×10^{19} cm^{-3} for the sample implanted with 10^{16} cm^{-2} and a higher value of 3.93×10^{20} cm^{-3} for sample implanted with 10^{15} cm^{-3}. In fact, the ratio of these impurities concentrations values is equal to 37.8, similar to the ratio of the scattering prefactor J of 32.4, in accordance with the predictions of Kondo's theory.

5. Conclusions

In conclusion, we have observed the insulator-to-metal transition in vanadium supersaturated silicon samples obtained by the use of ion implantation and PLM techniques. Samples with a vanadium concentration below and over the theoretical n_{crit} present a high quality single crystal. By means of an exhaustive electrical transport analysis we have identified that the insulator-to-metal transition occurs at a vanadium concentration between 1.1×10^{20} and 1.3×10^{21} cm^{-3}. At vanadium concentration just below the transition, electrical transport is defined by a variable-range hopping process with a Coulomb gap in the density of states. The electron-wavefunction localization length increases as the vanadium concentration increases for samples in the insulating phase, confirming the theory prediction of deep-levels delocalization process. Those samples in the metallic phase present a scattering process dominated by the Kondo effect, suggesting the presence of local magnetic moments due to the *d*-levels of vanadium atoms.

Acknowledgments

Authors would like to acknowledge the CAI de Técnicas Físicas of the Universidad Complutense de Madrid for the ion implantation procees and metallic evaporations. This work was partially supported by the Project MADRID-PV (Grant No. 2013/MAE-2780) funded by the Comunidad de Madrid, by the Spanish MINECO (Economic and Competitiviness Ministery) under grant TEC 2013-41730-R and by the Universidad Complutense de Madrid (Programa de Financiación de Grupos de Investigación UCM-Banco Santander) under grant 910173-2014. D Montero acknowledge the Spanish MINECO (Economic and Competitiviness Ministery) for financial support under contract BES-2014-067585.

AQ3

AQ4 ## References

[1] Zheng H and Wagner L K 2015 *Phys. Rev. Lett.* **114** 176401
[2] Brzezicki W, Noce C, Romano A and Cuoco M 2015 *Phys. Rev. Lett.* **114** 247002
[3] Fuhr J D, Avignon M and Alascio B 2008 *Phys. Rev. Lett.* **100** 216402
[4] Shlimak I and Kaveh M 1998 *Phys. Rev.* B **58** 15333
[5] Hammer D, Wu J and Leighton C 2004 *Phys. Rev.* B **69** 134407
[6] Seo Y, Qin Y, Vicente C L, Choi K S and Yoon J 2006 *Phys. Rev. Lett.* **97** 057005
[7] Edwards P P and Sienko M J 1978 *Phys. Rev.* B **17** 2575
[8] Neamen D A 1997 *Semiconductor Physics and Devices* (Irwin)
AQ5
[9] Rosenbaum T F, Milligan R F, Paalanen M A, Thomas G A, Bhatt R N and Lin W 1983 *Phys. Rev.* B **27** 7509
[10] Luque A, Marti A, Antolin E and Tablero C 2006 *Phys. B: Condens. Matter* **382** 320
[11] Pastor D, Olea J, del Prado A, Garcia-Hemme E, Garcia-Hernansanz R and Gonzalez-Diaz G 2012 *Sol. Energy Mater. Sol. Cells* **104** 159
[12] Winkler M T, Recht D, Sher M-J, Said A J, Mazur E and Aziz M J 2011 *Phys. Rev. Lett.* **106** 178701
[13] Olea J, Toledano-Luque M, Pastor D, Gonzalez-Diaz G and Martil I 2008 *J. Appl. Phys.* **104**
[14] Tabbal M, Kim T, Woolf D N, Shin B and Aziz M J 2010 *Appl. Phys.* A **98** 589
[15] Garcia-Hemme E, Garcia-Hernansanz R, Olea J, Pastor D, del Prado A, Martil I and Gonzalez-Diaz G 2014 *Appl. Phys. Lett.* **104** 211105
[16] Garcia-Hemme E, Garcia-Hernansanz R, Olea J, Pastor D, del Prado A, Martil I and Gonzalez-Diaz G 2013 *Appl. Phys. Lett.* **103** 032101
[17] Luque A and Marti A 1997 *Phys. Rev. Lett.* **78** 5014
[18] Luque A, Marti A and Stanley C 2012 *Nat. Photon.* **6** 146
[19] Pastor D, Olea J, del Prado A, Garcia-Hemme E, Garcia-Hernansanz R, Martil I and Gonzalez-Diaz G 2013 *J. Phys. D: Appl. Phys.* **46**
[20] Olea J, Pastor D, Toledano-Luque M, Martil I and Gonzalez-Diaz G 2011 *J. Appl. Phys.* **110** 064501
[21] Narayan J, White C W, Aziz M J, Stritzker B and Walthuis A 1985 *J. Appl. Phys.* **57** 564
[22] Tsouroutas P, Tsoukalas D, Zergioti I, Cherkashin N and Claverie A 2009 *J. Appl. Phys.* **105** 094910
[23] Pastor D, Olea J, Munoz-Martin A, Climent-Font A, Martil I and Gonzalez-Diaz G 2012 *J. Appl. Phys.* **112** 113514
[24] Sriranganathan R, Wollkind D J and Oulton D B 1983 *J. Cryst. Growth* **62** 265
[25] Cullis A G, Hurle D T J, Webber H C, Chew N G, Poate J M, Baeri P and Foti G 1981 *Appl. Phys. Lett.* **38** 642
[26] Akey A J, Recht D, Williams J S, Aziz M J and Buonassisi T 2015 *Adv. Funct. Mater.* **25** 4642
[27] Pastor D, Olea J, del Prado A, Garcia-Hemme E, Martil I, Gonzalez-Diaz G, Ibanez J, Cusco R and Artus L 2011 *Semicond. Sci. Technol.* **26**
AQ6
[28] Luque A and Marti A 2011 *Nat. Photon.* **5** 137
[29] Dai P H, Zhang Y Z and Sarachik M P 1992 *Phys. Rev.* B **45** 3984
[30] Castner T G 1991 *Hopping Transport in Solids* (Amsterdam: Elsevier)
[31] Zabrodskii A G and Zinoveva K N 1983 *J. Exp. Theor. Phys. Lett.* **37** 436
[32] Lee P A and Ramakrishnan T V 1985 *Rev. Mod. Phys.* **57** 287
[33] Altshuler B L and Aronov A G 1979 *J. Exp. Theor. Phys. Lett.* **30** 482
[34] xxxx
AQ7
[35] Efros A L and Shklovskii B I 1975 *J. Phys. C: Solid State Phys.* **8** L49
[36] Mott N F 1968 *Rev. Mod. Phys.* **40** 677
[37] Ishida S, Takaoka S, Murase K, Shirai S and Serikawa T 1994 *J. Phys. Soc. Japan* **63** 1254
[38] Hewson A C 1993 *The Kondo Problem to Heavy Fermions* (Cambridge: Cambridge University Press)
[39] Feng X G, Popovic D, Washburn S and Dobrosavljevic V 2001 *Phys. Rev. Lett.* **86** 2625
[40] Kondo J 1964 *Prog. Theor. Phys.* **32** 37

QUERIES

Page 1
AQ1
Please provide the e-mail address for the corresponding author.
AQ2
Please be aware that the colour figures in this article will only appear in colour in the online version. If you require colour in the printed journal and have not previously arranged it, please contact the Production Editor now.
Page 7
AQ3
We have been provided funding information for this article as below. Please confirm whether this information is correct.
1. Comunidad de Madrid: 2013/MAE-2780; 2. Universidad Complutense de Madrid: 910173-2014; 3. Ministerio de Economía y Competitividad: BES-2014-067585, TEC 2013-41730-R.
AQ4
Please check the details for any journal references that do not have a link as they may contain some incorrect information.
AQ5
Please provide the publisher location for reference [8].
AQ6
Please provide the page/article number for reference [27].
AQ7
Reference [34] is cited in text but not provided in the list. Please provide complete publication details to insert in the list, else delete the citation from the text.